Ground-state properties of doubly magic nuclei from the unitary-model-operator approach with chiral two- and three-nucleon forces

T. Miyagi, T. Abe, M. Kohno, P. Navrátil, R. Okamoto, T. Otsuka, N. Shimizu, and S. R. Stroberg

Phys. Rev. C **100**, 034310 — Published 13 September 2019

DOI: 10.1103/PhysRevC.100.034310

Ground-state properties of doubly magic nuclei from the unitary-model-operator approach with chiral two- and three-nucleon forces

T. Miyagi,[1,2] T. Abe,[3,1] M. Kohno,[4] P. Navrátil,[2] R. Okamoto,[5]
T. Otsuka,[6,3,7,8] N. Shimizu,[1] and S. R. Stroberg[2,9,10]

[1] *Center for Nuclear Study, The University of Tokyo, 7-3-1 Hongo, Bunkyo, Tokyo 113-0033, Japan*
[2] *TRIUMF, 4004 Wesbrook Mall, Vancouver, British Columbia, V6T 2A3 Canada*
[3] *Department of Physics, The University of Tokyo, 7-3-1, Hongo, Bunkyo, Tokyo 113-0033, Japan*
[4] *Research Center for Nuclear Physics, Osaka University, Japan*
[5] *Senior Academy, Kyushu Institute of Technology, Tobata, Kitakyushu 804-0015, Japan*
[6] *RIKEN Nishina Center, 2-1 Hirosawa, Wako, Saitama 351-0198, Japan*
[7] *National Superconducting Cyclotron Laboratory, Michigan State University, East Lansing, Michigan 48824, USA*
[8] *Instituut voor Kern- en Stralingsfysica, KU Leuven, B-3001 Leuven, Belgium*
[9] *Physics Department, Reed College, Portland, Oregon, 97202 USA*
[10] *Department of Physics, University of Washington, Seattle WA 98195, USA*

(Dated: June 20, 2019)

The ground-state energies and radii for ^{4}He, ^{16}O, and ^{40}Ca are calculated with the unitary-model-operator approach (UMOA). In the present study, we employ similarity renormalization group (SRG) evolved nucleon-nucleon (NN) and three-nucleon ($3N$) interactions based on chiral effective field theory. This is the first UMOA calculation with both NN and $3N$ interactions. The calculated ground-state energies and radii are consistent with the recent *ab initio* results with the same interaction. We evaluate the expectation values of two- and three-body SRG evolved radius operators, in addition to those of the bare radius operator. With the aid of the higher-body evolution of the radius operator, it is seen that the calculated radii tend to be SRG resolution-scale independent. We find that the SRG evolution gives minor modifications for the radius operator.

I. INTRODUCTION

Recent nuclear *ab initio* studies are encouraged by the development, in particular, of nuclear interactions from the chiral effective field theory (χEFT) [1, 2]. In χEFT, nuclear interactions are obtained through the low-momentum expansion of the chiral Lagrangian which is the effective Lagrangian of quantum chromodynamics. By taking into account higher-order expansion terms, the systematic improvement of the nuclear interactions can be expected (for recent example, see Refs. [3–5]). As another advantage, χEFT allows for the systematic derivation of the three-nucleon ($3N$) interaction. With the development of χEFT interactions, the impacts of the $3N$ force on nuclear structure calculation have been discussed extensively, for example, in light nuclei [6–9], medium-mass nuclei [10–18], and infinite nuclear matter [19–22].

Besides the progress in nuclear forces, advances in many-body methods are also necessary. To deal with nuclear many-body problems, one can use the *ab initio* calculation methods such as no-core shell model (NCSM) [23], quantum Monte Carlo methods [24], nuclear lattice EFT calculations [25], coupled-cluster method [26], self-consistent Green's function method [27], in-medium similarity renormalization group approach [28], and many-body perturbation theory [29, 30]. Over the past decade, much effort has been made in nuclear *ab initio* studies. The capability of the *ab initio* calculations has reached mass region $A \sim 100$ [18, 29, 31]. Another alternative to these methods is the unitary-model-operator approach (UMOA) [32, 33]. In the UMOA, a unitary transformation of the Hamiltonian is constructed so that the one-particle-one-hole and two-particle-two-hole excitations do not occur. So far, we have calculated the ground-state energies and radii for some closed shell nuclei with only the nucleon-nucleon (NN) interactions [33]. In this work, we include $3N$ interactions in the UMOA for the first time.

Due to the non-perturbative nature of the nuclear force, in most cases it is not possible to apply directly the nuclear interactions to the many-body calculations. To bridge the gap between nuclear forces and many-body calculations, we evolve the nuclear Hamiltonian with the similarity renormalization group (SRG) flow equation [34]. Through the SRG evolution, we obtain the Hamiltonian whose coupling between low- and high-momentum states is suppressed. With such nuclear interactions, recent *ab initio* results significantly underestimate the nuclear radii, see for instance Refs. [16, 17, 28, 35]. Since the nuclear size can affect the single-particle level structure of a nucleus, the reproduction of nuclear radii is one of the fundamental issues to discuss the nuclear structure. As seen in NCSM calculations for few-body systems [36, 37], one should also evolve other operators consistently with the Hamiltonian. In this work, we demonstrate the effect of the SRG evolution on the radius operator.

This paper is organized as follows. The Hamiltonian and radius operators employed in this work are introduced in Sec. II. Section III briefly describes the formalism of the UMOA. In Sec. IV, numerical results for ^{4}He, ^{16}O, and ^{40}Ca are given. After confirming convergence and consistency with the other *ab initio* results, the ef-

fects of the SRG evolution on the radius operator are discussed. The summary of the present work is given in Sec. V.

II. HAMILTONIAN AND RADIUS OPERATORS

Our starting Hamiltonian is composed of the kinetic, NN, and $3N$ terms:

$$H = T + V^{NN} + V^{3N}. \tag{1}$$

Here, T is the kinetic energy operator and V^{NN} and V^{3N} indicate the NN and $3N$ interactions, respectively. Usually, the bare Hamiltonian H is too hard for use in the many-body calculation. It causes slow convergence with respect to the size of model space and calculations demand a huge amount of computational resources. To obtain converged results from feasible model space, similarity-renormalization group (SRG) evolution [34] is employed in this work. We consider a unitary transformation of the original Hamiltonian:

$$H(\alpha) = U^{\dagger}_{\rm SRG}(\alpha) H U_{\rm SRG}(\alpha). \tag{2}$$

Here, $U_{\rm SRG}(\alpha)$ is the unitary transformation operator and is evolved by the flow equation:

$$\frac{dU_{\rm SRG}(\alpha)}{d\alpha} = U_{\rm SRG}(\alpha)\eta(\alpha) \tag{3}$$

and α is the resolution scale parameter of the flow equation in units of fm^4. η is called the generator of the SRG evolution and is taken as $\eta(\alpha) = [T, H(\alpha)]$. Note that the initial condition for $U_{\rm SRG}(\alpha)$ is $U_{\rm SRG}(0) = \mathbb{1}$. As an alternative to α, it is common to use $\lambda_{\rm SRG} = \alpha^{-1/4}$ for controlling the flow equation Eq. (3). The Hamiltonian is transformed by Eq. (2) from $\lambda_{\rm SRG} = \infty$ fm^{-1} to lower values where the interaction is soft enough to enable convergence of the many-body calculation methods. As discussed, for example in Ref. [38], the SRG evolution induces the many-body forces:

$$H(\lambda_{\rm SRG}) = T + V^{NN}(\lambda_{\rm SRG}) + V^{3N}(\lambda_{\rm SRG}) + \cdots. \tag{4}$$

Consequently, during the SRG evolution, one should keep many-body terms, even if the starting Hamiltonian does not include many-body interactions. In this work, three types of Hamiltonians are used. The first one, labeled by NN–only, is obtained by keeping only the NN interaction during the SRG evolution, starting without the genuine $3N$ interaction. The second one, $NN+3N$–ind is obtained by keeping the NN and $3N$ interactions during the SRG evolution, starting without the genuine $3N$ interaction. The third one, $NN+3N$–full is obtained by keeping the NN and $3N$ interactions during the SRG evolution, starting with the genuine $3N$ interaction.

To evaluate nuclear root-mean-squared radii, we transform the radius operator in the same manner as the Hamiltonian:

$$r^2(\alpha) = U^{\dagger}_{\rm SRG}(\alpha) r^2 U_{\rm SRG}(\alpha). \tag{5}$$

The original radius operator is defined as

$$r^2 = r^{2(2)} = \frac{1}{A^2}\sum_{i<j}(\mathbf{r}_i - \mathbf{r}_j)^2 \tag{6}$$

with the coordinate vector of the i–th nucleon $\mathbf{r}_i$ and number of nucleons A. In the same manner as the Hamiltonian, many-body contributions to the radius operator can be induced through the SRG evolution:

$$r^2(\lambda_{\rm SRG}) = r^{2(2)}(\lambda_{\rm SRG}) + r^{2(3)}(\lambda_{\rm SRG}) + \cdots. \tag{7}$$

Following to Refs. [36, 37], we keep up to three-body terms.

To perform many-body calculations, it is numerically efficient to transform to the laboratory frame. Then, our Hamiltonian and radius operators can be rewritten as

$$H = T^{(1)} + [T^{(2)} + V^{NN}(\lambda_{\rm SRG})] + V^{3N}(\lambda_{\rm SRG}), \tag{8}$$
$$r^2 = r^{2(1)} + [r^{2(2)}(\lambda_{\rm SRG}) - r^{2(1)}] + r^{2(3)}(\lambda_{\rm SRG}). \tag{9}$$

Here, we use $T^{(1)} = \sum_i (1-1/A)\mathbf{p}_i^2/2m$ with the i–th nucleon momentum $\mathbf{p}_i$ and nucleon mass m, $T^{(2)} = -\sum_{i<j}\mathbf{p}_i\cdot\mathbf{p}_j/mA$, and $r^{2(1)} = (1-1/A)\sum_i \mathbf{r}_i^2$. Note that $r^{2(1)}$ is chosen so that $r^{2(2)}(\lambda_{\rm SRG}) - r^{2(1)}$ goes to $-\sum_{i<j}\mathbf{r}_i\cdot\mathbf{r}_j/A$ in the limit of $\lambda_{\rm SRG}\to\infty$. In second quantization form, an operator is

$$\begin{aligned} O = &\sum_{a_1 a_2} o_{a_1 a_2} c^{\dagger}_{a_1} c_{a_2} \\ &+ \left(\frac{1}{2!}\right)^2 \sum_{a_1 a_2 a_3 a_4} o^{(2)}_{a_1 a_2 a_3 a_4} c^{\dagger}_{a_1} c^{\dagger}_{a_2} c_{a_4} c_{a_3} \\ &+ \left(\frac{1}{3!}\right)^2 \sum_{a_1 a_2 a_3 a_4 a_5 a_6} o^{(3)}_{a_1 a_2 a_3 a_4 a_5 a_6} c^{\dagger}_{a_1} c^{\dagger}_{a_2} c^{\dagger}_{a_3} c_{a_6} c_{a_5} c_{a_4}. \end{aligned} \tag{10}$$

Here, c_a ($c^{\dagger}_a$) is the annihilation (creation) operator of the nucleon at the state a. In Eq. (10), the matrix elements are

$$o^{(1)}_{a_1 a_2} = \langle a_1 | T^{(1)} | a_2 \rangle, \tag{11}$$
$$o^{(2)}_{a_1 a_2 a_3 a_4} = \langle a_1 a_2 | V^{NN}(\lambda_{\rm SRG}) + T^{(2)} | a_3 a_4 \rangle, \tag{12}$$
$$o^{(3)}_{a_1 a_2 a_3 a_4 a_5 a_6} = \langle a_1 a_2 a_3 | V^{3N}(\lambda_{\rm SRG}) | a_4 a_5 a_6 \rangle, \tag{13}$$
$$\tag{14}$$

for the Hamiltonian, with analogous expressions for the radius operator. Because of the computational limitation, however, the direct treatment of the three-body matrix elements is still challenging. Therefore, we follow the recent nuclear *ab initio* studies and introduce the normal-ordered two-body (NO2B) approximation [39, 40]. The

key of the approximation is a rearrangement of the three-body term with respect to a reference state $|\Phi\rangle$. After the rearrangement, one obtains zero-, one-, two-, and three-body terms. In the NO2B approximation, the residual three-body part is discarded. To apply to the UMOA framework, we take normal order again with respect to the nucleon vacuum state. Then, the operator can be approximated as

$$O \approx o^{(0),\mathrm{NO2B}} + \sum_{a_1 a_2} o^{(1),\mathrm{NO2B}}_{a_1 a_2} c^\dagger_{a_1} c_{a_2} + \left(\frac{1}{2!}\right)^2 \sum_{a_1 a_2 a_3 a_4} o^{(2),\mathrm{NO2B}}_{a_1 a_2 a_3 a_4} c^\dagger_{a_1} c^\dagger_{a_2} c_{a_4} c_{a_3} \tag{15}$$

The matrix elements are

$$o^{(0),\mathrm{NO2B}} = \frac{1}{6} \sum_{abc} v^{(3)}_{abcabc} n_a n_b n_c, \tag{16}$$

$$o^{(1),\mathrm{NO2B}}_{a_1 a_2} = t_{a_1 a_2} - \frac{1}{2} \sum_{bc} v^{(3)}_{a_1 bc a_2 bc} n_b n_c, \tag{17}$$

$$o^{(2),\mathrm{NO2B}}_{a_1 a_2 a_3 a_4} = v^{(2)}_{a_1 a_2 a_3 a_4} + \sum_{b} v^{(3)}_{a_1 a_2 b a_3 a_4 b} n_b. \tag{18}$$

for the Hamiltonian, with analogous expressions for the radius operator. Here, n_a is an occupation number for the orbit a, i.e. $n_a = 1$ ($n_a = 0$) where a is below (above) the Fermi level. To minimize the effect of the truncated residual three-body term, the choice of $|\Phi\rangle$ is crucial. In this work, we use the Hartree-Fock ground state as $|\Phi\rangle$.

III. UNITARY-MODEL-OPERATOR APPROACH

To solve the many-body Schrödinger equation associated with the Hamiltonian Eq. (15), the UMOA [32, 33, 42, 43] is employed in this work. In the UMOA, we construct the effective Hamiltonian with the unitary transformation:

$$\widetilde{H} = U^\dagger H U. \tag{19}$$

The operator U is defined as the product of two exponential operators,

$$U = e^{S^{(1)}} e^{S^{(2)}}, \tag{20}$$

where $S^{(1)}$ and $S^{(2)}$ are anti-hermitian one- and two-body correlation operators, respectively. Note that the sole use of $S^{(1)}$ ($S^{(2)} = 0$) reduces the UMOA to Hartree-Fock (HF) theory. $S^{(1)}$ and $S^{(2)}$ are specified by iteratively applying the Okubo-Lee-Suzuki method [44–46] so that $\widetilde{H}$ does not induce one-particle-one-hole and two-particle-two-hole excitations from the reference state $|\Phi\rangle$. Since the unitary transformation (19) can induce many-body interactions, $\widetilde{H}$ can include many-body operators even if the original Hamiltonian is restricted up to the two-body interaction. In actual calculations, we decompose $\widetilde{H}$ with the cluster expansion and truncate the effect of the four- and higher-body cluster terms:

$$\widetilde{H} \approx \sum_{a_1 a_2} \widetilde{H}^{(1)}_{a_1 a_2} c^\dagger_{a_1} c_{a_2} + \frac{1}{4} \sum_{a_1 a_2 a_3 a_4} \widetilde{H}^{(2)}_{a_1 a_2 a_3 a_4} c^\dagger_{a_1} c^\dagger_{a_2} c_{a_4} c_{a_3} + \frac{1}{36} \sum_{a_1 a_2 a_3 a_4 a_5 a_6} \widetilde{H}^{(3)}_{a_1 a_2 a_3 a_4 a_5 a_6} c^\dagger_{a_1} c^\dagger_{a_2} c^\dagger_{a_3} c_{a_6} c_{a_5} c_{a_4}, \tag{21}$$

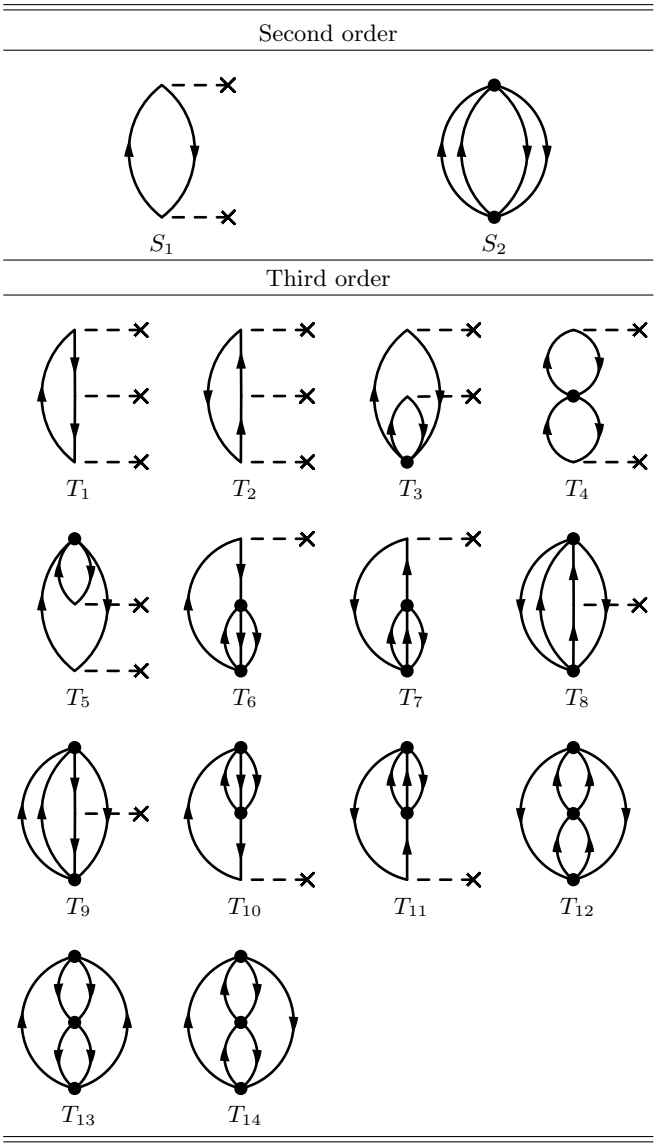

FIG. 1. Hugenholtz diagrams for the ground-state energy up to the third order. Note that the first order contributions are omitted. The cross and dot indicate the one- and two-body part of Hamiltonian, respectively. The diagram rules are same as in Ref. [41].

where $\widetilde{H}^{(1)}_{a_1a_2}$, $\widetilde{H}^{(2)}_{a_1a_2a_3a_4}$, and $\widetilde{H}^{(3)}_{a_1a_2a_3a_4a_5a_6}$ are the one-, two-, and three-body matrix elements, respectively (see Ref. [33] for more details). The ground-state energy $E_{\rm g.s.}$ is approximately

$$E_{\rm g.s.} \approx E^{\rm 1,2BC} + E^{\rm 3BC}, \tag{22}$$

$$E^{\rm 1,2BC} = \sum_a \widetilde{H}^{(1)}_{aa} n_a + \frac{1}{2}\sum_{ab} \widetilde{H}^{(2)}_{abab} n_a n_b, \tag{23}$$

$$E^{\rm 3BC} = \frac{1}{6}\sum_{abc} \widetilde{H}^{(3)}_{abcabc} n_a n_b n_c. \tag{24}$$

Since direct treatment of the three-body term demands huge computational resources, the contribution of three-body cluster term is approximately evaluated up to second order in $S^{(2)}$ [32]:

$$E^{\rm 3BC} \approx \frac{1}{4}\sum_{abcd}\sum_{ef} \widetilde{H}^{(2)}_{abcd} S^{(2)}_{efab} S^{(2)}_{efcd} n_a n_b n_c n_d \bar{n}_e \bar{n}_f + \sum_{abc}\sum_{def} \widetilde{H}^{(2)}_{adcf} S^{(2)}_{debc} S^{(2)}_{efab} n_a n_b n_c \bar{n}_d \bar{n}_e \bar{n}_f. \tag{25}$$

$S^{(2)}_{abcd}$ is the matrix element of the two-body correlation operator and $\bar{n}_a = 1 - n_a$ is used. To clarify the contribution of each cluster term, it is useful to compare with many-body perturbation theory (MBPT). Figure 1 shows the diagrams for the ground-state energy from the third-order MBPT. Following to the perturbative derivation of correlation operators, shown for example in Refs [47, 48], the contribution of each cluster term to the ground-state energy can be derived. In terms of the many-body perturbation theory, $E^{\rm 1,2BC}$, $E^{\rm 3BC}$, and $E_{\rm g.s.}$ are

$$E^{\rm 1,2BC} = E_1 + \sum_{i=1}^{2} S_i + \sum_{i=1}^{12} T_i - T_{13} + (\text{higher order terms}), \tag{26}$$

$$E^{\rm 3BC} = 2T_{13} + T_{14} + (\text{higher order terms}), \tag{27}$$

$$E_{\rm g.s.} = E_1 + \sum_{i=1}^{2} S_i + \sum_{i=1}^{14} T_i + (\text{higher order terms}). \tag{28}$$

Here, S_i and T_i are the second- and third-order contributions shown in Fig 1, respectively, and E_1 is the first order ground-state energy. At the one-plus-two-body cluster level, the third-order diagrams are not complete. The three-body cluster term contributions compensate the third order [49]. Note that S_1 and T_1 to T_{11} vanish when the HF basis is employed. Since the other *ab initio* methods also complete up to the third order, it is useful to investigate fourth order contributions taken into account in the UMOA. The fourth order contributions assuming the HF basis are discussed in Appendix A.

To evaluate the expectation value of the radius operator, the effective operator $\widetilde{r}^2$ is used:

$$\widetilde{r}^2 = U^\dagger r^2 U. \tag{29}$$

Similarly to the Hamiltonian, the unitary transformation of the radius operator induces the many-body terms. However, results examined here are calculated keeping up to two-body terms and does not include any contributions from three- and higher-body terms [33]:

$$\widetilde{r}^2 \approx \sum_{a_1a_2} \widetilde{r}^{2(1)}_{a_1a_2} c^\dagger_{a_1} c_{a_2} + \frac{1}{4}\sum_{a_1a_2a_3a_4} \widetilde{r}^{2(2)}_{a_1a_2a_3a_4} c^\dagger_{a_1} c^\dagger_{a_2} c_{a_4} c_{a_3}. \tag{30}$$

Then, the mean-squared radius $r^2_{\rm g.s.}$ is approximately evaluated as

$$r^2_{\rm g.s.} \approx \sum_a \widetilde{r}^{2(1)}_{aa} n_a + \frac{1}{2}\sum_{ab} \widetilde{r}^{2(2)}_{abab} n_a n_b. \tag{31}$$

IV. RESULTS AND DISCUSSIONS

In this work, we use the next-to-next-to-next-to leading order ($\rm N^3LO$) NN interaction by Entem and Machleidt [51] and local form $\rm N^2LO$ $3N$ interaction [52] from χEFT. Both two- and three-body SRG evolutions are done in the harmonic-oscillator (HO) space. The two-body interactions are obtained from the $N_{\rm max} = 200$ space calculations. Here, $N_{\rm max}$ is the boundary of the HO quantum number for the two-body relative coordinate and is $N_{\rm max} = \max(2n+l)$ with the radial quantum number n and angular momentum l. Following Ref. [53], the three-body SRG evolution is done in ramp A model space defined in Fig. 3 in Ref [53]. To obtain the three-body matrix element, the frequency conversion technique [53] is used with the parent HO energy $\hbar\omega = 35$ MeV matrix elements. For $\rm N^2LO$ $3N$ interaction, we use $c_D = -0.2$, $c_E = 0.098$, and $\Lambda_{3N} = 400$ MeV/c [39], so as to compare with the other *ab initio* calculation results. Note that the low-energy constant c_D used here does not fit the ^{3}H half-life as claimed in the past [54, 55]. The impact of the modification of the $3N$ force with the c_D that fits ^{3}H half-life will be discussed in the forthcoming publications. The size of the contributions from induced many-body forces can be estimated from the dependence of calculated results on the SRG resolution scale $\lambda_{\rm SRG}$. To do so, we employ three SRG resolution scales $\lambda_{\rm SRG} = 1.88$, 2.0, and 2.24 fm^{-1}. The NO2B approximated Hamiltonian is obtained through HF calculations at $e_{3\,\rm max} = 14$. Here, $e_{3\,\rm max}$ is introduced to handle the three-body matrix element and is $e_{3\,\rm max} = \max(2n_1+l_1+2n_2+l_2+2n_3+l_3)$ with the single-particle radial quantum number n_i ($i = 1, 2, 3$) and angular momentum l_i ($i = 1, 2, 3$). We checked that the changing from $e_{3\,\rm max} = 12$ to $e_{3\,\rm max} = 14$ changes the ground-state energy by less than 1%. UMOA calculations are done in the model space defined by $e_{\rm max} = \max(2n_1 + l_1)$ [33].

TABLE I. Ground-state energies for ^{4}He, ^{16}O, and ^{40}Ca. All the calculation results are obtained at $e_{\max} = 14$ and $\hbar\omega = 25$ MeV.

Nuclide	$\lambda_{\rm SRG}$ (fm^{-1})	$E_{\rm g.s.}$ (MeV)			
		NN–only	$NN+3N$–ind	$NN+3N$–full	Exp.[50]
^{4}He	1.88	−27.94	−25.19	−27.81	
	2.0	−27.73	−25.18	−27.76	−28.30
	2.24	−27.23	−25.16	−27.62	
^{16}O	1.88	−167.79	−119.33	−127.16	
	2.0	−162.69	−119.51	−126.33	−127.62
	2.24	−152.88	−119.56	−124.50	
^{40}Ca	1.88	−615.62	−349.08	−368.44	
	2.0	−588.45	−352.03	−366.14	−342.05
	2.24	−536.26	−355.61	−360.23	

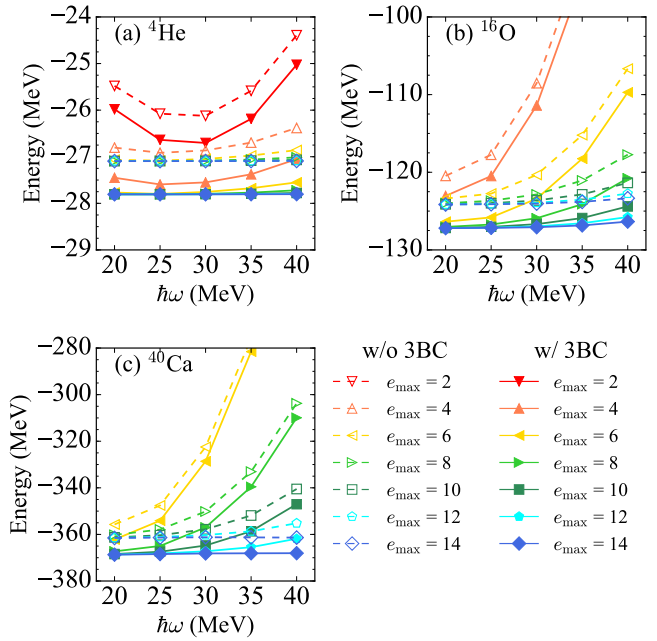

FIG. 2. (color online) Ground-state energies for ^{4}He, ^{16}O, and ^{40}Ca as functions of $\hbar\omega$ with the $NN+3N$–full interaction. The dashed (solid) lines calculated without (with) the three-body cluster term energy. The interaction is obtained by SRG evolution of chiral N^{3}LO NN [51] and N^{2}LO $3N$ [6, 39] interactions up to $\lambda_{\rm SRG} = 1.88$ fm^{-1}.

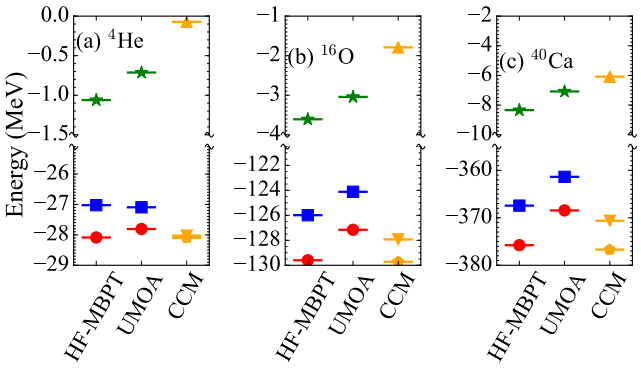

FIG. 3. (color online) Ground-state energies from the Hartree-Fock basis many-body perturbation theory (HF-MBPT), UMOA, and coupled-cluster method (CCM). The energies of HF-MBPT are calculated with Eqs. (32)-(34). The CCM results are taken from Refs. [18, 56]. The interaction is obtained by SRG evolution of chiral N^{3}LO NN [51] and N^{2}LO $3N$ [6, 39] interactions up to $\lambda_{\rm SRG} = 1.88$ fm^{-1}. For the HF-MBPT and UMOA energies, $E^{1,2\rm BC}$ (square), $E^{3\rm BC}$ (star), and $E_{\rm g.s.}$ (circle) are shown. For the CCM energies, CCSD (down triangle), triple correction (up triangle), and CR-CC(2,3) energies (pentagon) are shown.

A. Ground-state energies

Figure 2 shows the convergence of the ground-state energies for ^{4}He, ^{16}O, and ^{40}Ca calculated with the $NN+3N$–full interaction evolved to $\lambda_{\rm SRG} = 1.88$ fm^{-1}. Our calculations are done with varying $\hbar\omega$ and $e_{\max}$ to see the numerical convergence. Note that the final results should not depend on $\hbar\omega$ because the initial Hamiltonian Eq. (1) does not include $\hbar\omega$. Similar to other *ab initio* calculations, our ground-state energies show parabolic $\hbar\omega$-dependence at small $e_{\max}$ and gain with increasing $e_{\max}$. For all cases examined here, $\hbar\omega$- and $e_{\max}$-independent results are obtained in $e_{\max} = 14$. The results with $e_{\max} = 14$ and $\hbar\omega = 25$ MeV are used in the following discussion.

To investigate the role of each cluster term, the comparison between energies from UMOA, Hartree-Fock basis many-body perturbation theory (HF-MBPT), and coupled-cluster method (CCM) is illustrated in Fig. 3. In terms of HF-MBPT, the energies $E^{1,2\rm BC}_{\rm MBPT}$, $E^{3\rm BC}_{\rm MBPT}$, and

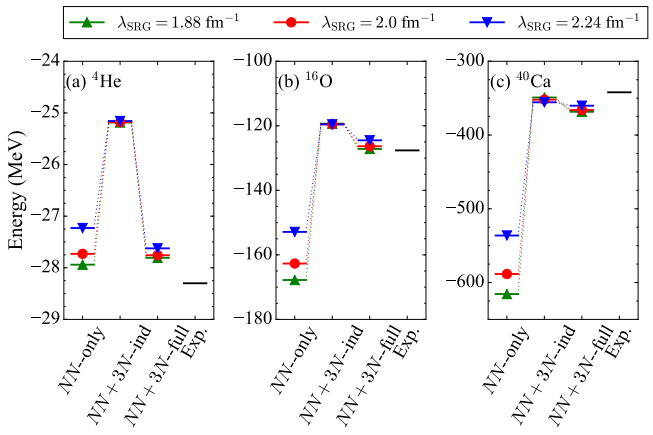

FIG. 4. (color online) Ground-state energies for ^{4}He, ^{16}O, and ^{40}Ca. All the calculation results are obtained at $e_{\max} = 14$ and $\hbar\omega = 25$ MeV. The experimental data are taken from Ref. [50]

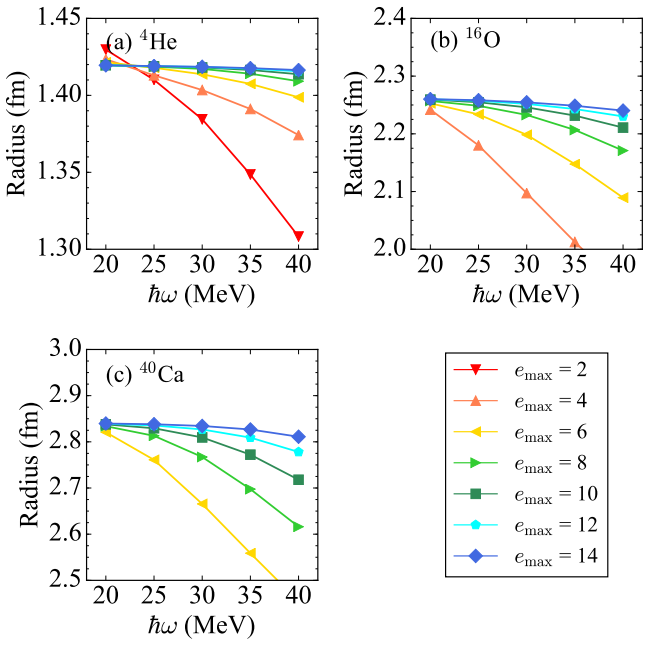

FIG. 5. (color online) Expectation values of bare root-mean-squared radius operator for ^{4}He, ^{16}O, and ^{40}Ca as functions of $\hbar\omega$. Here, $NN + 3N$–full interaction at $\lambda_{\rm SRG} = 1.88$ fm^{-1} is employed.

$E_{\rm g.s.,MBPT}$ are evaluated as

$$E^{1,2\rm BC}_{\rm MBPT} = E_{\rm HF} + S_2 + T_{12} - T_{13}, \quad (32)$$
$$E^{3\rm BC}_{\rm MBPT} = 2T_{13} + T_{14}, \quad (33)$$
$$E_{\rm g.s.,MBPT} = E_{\rm HF} + S_2 + T_{12} + T_{13} + T_{14}, \quad (34)$$

with the Hartree-Fock energy $E_{\rm HF}$. Note that $E_{\rm g.s.,MBPT}$ is the third-order HF-MBPT energy. In the figure, the UMOA and HF-MBPT energies are reasonably close to each other, and it can be seen that the main contributions of $E^{3\rm BC}$ are from the third order hole-hole (T_{13}) and particle-hole (T_{14}) ladder diagrams. Also, the sum of fourth order diagrams taken into account in the UMOA seems to be repulsive (see Appendix A for details). Comparing to CCM energies, total UMOA energies (circle) look closer to the CCSD energies (down triangle) than to the CR-CC(2,3) energies (pentagon). Note that the agreement of HF-MBPT and CR-CC(2,3) implies the non-trivial cancellations of higher order diagrams. The $E^{3\rm BC}$ are -0.71, -3.04, and -7.07 MeV for ^{4}He, ^{16}O, and ^{40}Ca, respectively, and are only a few percents of the total energies. Since the contributions from four- and higher-body cluster terms are expected to be smaller than those from the three-body cluster term, the UMOA results are converged with respect to the cluster expansion. For ^{16}O, our ground-state energy -127.16 MeV is slightly underbound compared to the experimental energy (-127.62 MeV), while the recent *ab initio* calculation results show mildly overbound to the experiment, for example, $-130.6(1)$ MeV from in-medium SRG approach [14] and -129.7 MeV from CCM [18]. Again, this disagreement between our and other *ab initio* results is same order of magnitude as the perturbative three-body-cluster contribution and consistent with the expected accuracy of the UMOA calculations.

As for calculations with NN–only and $NN + 3N$–ind interactions, we observe the similar convergence pattern and find the converged results at $e_{\max} = 14$ calculations. In Figure 4, the calculated ground-state energies are summarized together with the comparisons to the experimental data. In the case of the NN–only interaction, as the mass number increases, the ground-state energies show overbinding and $\lambda_{\rm SRG}$-dependence becomes considerable. By taking the SRG induced $3N$ interaction into account, the $\lambda_{\rm SRG}$-dependence is drastically reduced and ground-state energies rise. This $\lambda_{\rm SRG}$-independence of ground-state energies implies that the contributions from SRG induced four- and many-body interactions are negligible. With the genuine χEFT N^{2}LO $3N$ interaction, the calculated ground-state energies are comparable to the experimental data for ^{4}He and ^{16}O, while overbinding is seen for ^{40}Ca. The current choice of the genuine $3N$ interaction gives 9%, 6%, and 4% attractions for ^{4}He, ^{16}O, and ^{40}Ca, respectively. The energies presented in Fig. 4 are also displayed in Table I. Our ground-state energies show reasonable agreement with the other *ab initio* results from the same interaction [14, 16, 29, 39, 40, 57]. The explicit treatment of the three-body cluster term seems to be necessary to discuss more precisely the accuracy of the UMOA calculation. Such work is ongoing and will be reported in a future publication.

B. Root-mean square radii

In the same manner as the ground-state energy calculations, we calculate the expectation values of the

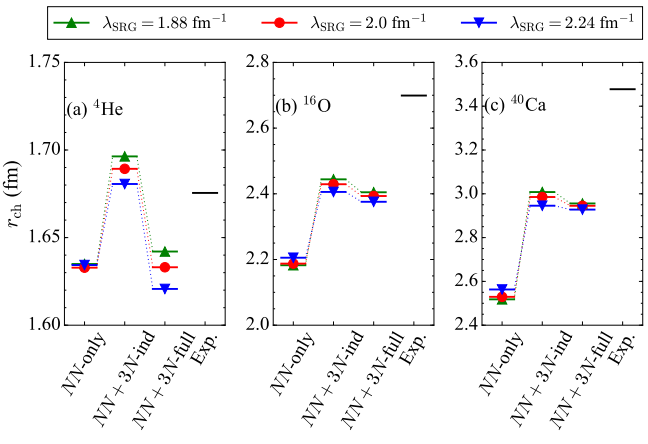

FIG. 6. (color online) Charge radii for ^{4}He, ^{16}O, and ^{40}Ca. All calculation results are obtained at $\hbar\omega = 25$ MeV and $e_{\rm max} = 14$. To evaluate the charge radii, the bare mean-squared radius operators are used. The experimental data are taken from Ref. [58].

bare root-mean-squared radius operator with the chiral $NN+3N$–full interaction at $\lambda_{\rm SRG} = 1.88$ fm $^{-1}$ varying both $\hbar\omega$ and $e_{\rm max}$ to examine the convergence. The results for ^{4}He, ^{16}O, and ^{40}Ca are illustrated in Fig. 5. As demonstrated in the figure, calculated radii become $\hbar\omega$- and $e_{\rm max}$-independent with increasing $e_{\rm max}$. At $\hbar\omega = 25$ MeV, we find the converged radii within 0.01 fm for all nuclei calculated here. Note that our converged radius of 2.84 fm for ^{40}Ca from the interaction evolved up to $\lambda_{\rm SRG} = 2.0$ fm^{-1} shows reasonable agreement with the SCGF result of 2.89 fm [16] with the same interaction.

We also calculate radii for ^{4}He, ^{16}O, and ^{40}Ca with the NN–only and $NN+3N$–ind interactions in the same manner as with the $NN+3N$–full interaction. Then, we find converged results at $e_{\rm max} = 14$ and $\hbar\omega = 25$ MeV within 0.01 fm. The results are summarized in Fig. 6 with the comparison to the experimental charge radii [58]. To compare with the experimental charge radii, our charge radii $r_{\rm ch}$ are evaluated as [59],

$$r_{\rm ch}^2 = r_{\rm g.s.}^2 + r_{\rm p}^2 + \frac{N}{Z} r_{\rm n}^2 + \frac{3}{4m^2}. \qquad (35)$$

Here, we use $r_{\rm p} = 0.8751(61)$ fm [60], $r_{\rm n}^2 = -0.1161(22)$ fm^2 [60], and $3/4m^2 = 0.033$ fm^2, with the averaged nucleon mass $m = 938.919$ MeV/c^2. Note that we assume the equivalence of point-proton and point-nucleon distributions in Eq. (35). This assumption is reasonable because our targets are $N = Z$ stable nuclei. In Fig. 7, the charge radii from NN–only interactions are obviously smaller than experimental data, especially for ^{16}O and ^{40}Ca, and consistent with overbinding ground-state energies from those. The SRG-induced three-body operator acts to spread the nuclear distribution out, and the $\lambda_{\rm SRG}$-dependence is slightly enhanced. With this particular Hamiltonian, the genuine $3N$ interaction shrinks nuclei and the calculated radii are clearly smaller than

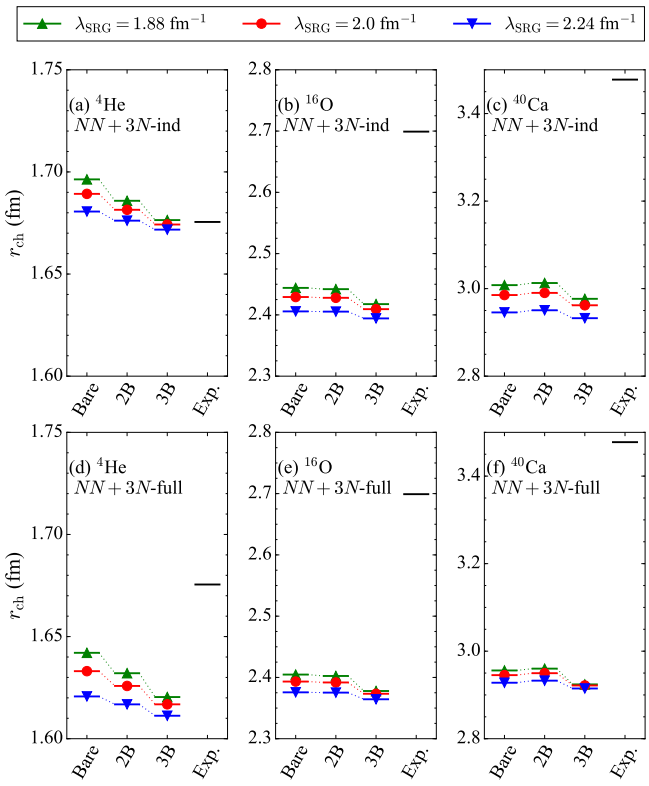

FIG. 7. (color online) Charge radii evaluated with the expectation values of bare, two-body (2B) SRG evolved, and three-body (3B) SRG evolved mean-squared radius operator for ^{4}He [(a) and (d)], ^{16}O [(b) and (e)], and ^{40}Ca [(c) and (f)]. All calculation results are obtained at $\hbar\omega = 25$ MeV and $e_{\rm max} = 14$. The calculation results in panels (a), (b), and (c) are calculated with $NN+3N$–ind interactions and the calculation results in panels (d), (e), and (f) are calculated with $NN+3N$–full interactions.

the experimental data.

One possible reason for the small calculated radii is the employed nuclear interaction. In fact, the simultaneous reproduction of ground-state energies and radii were accomplished with a χEFT N^{2}LO $NN+3N$ interaction fitted by using some selected data of nuclei up to $A = 25$ [61]. In addition, the saturation property of infinite nuclear matter was reproduced with the combinations of the softened N^{3}LO NN and bare N^{2}LO $3N$ interactions whose low-energy constants are fitted to reproduce data of the few body systems [19]. The ground-state energies and radii for finite nuclei with such interactions were discussed in Ref. [62]. As another possibility, we can consider amending the treatment of radius operator [63]. In earlier no-core shell model (NCSM) studies [36, 37], the effect of the SRG evolution to several operators was investigated for few-body systems. However, such effects for medium-mass nuclei have not been clarified yet. In this work, we investigate the effect of the SRG evolution of the radius operator.

We calculate the expectation value with the bare, two-

TABLE II. Root-mean-squared radii $r_{\rm g.s.}$ for ^{4}He, ^{16}O, and ^{40}Ca calculated with the bare, two-body evolved (2B), and three-body evolved (3B) radius operators. The results from both NN+3N–ind and NN+3N–full are displayed. All the calculation results are obtained at $e_{\rm max} = 14$ and $\hbar\omega = 25$ MeV.

		$r_{\rm g.s.}$ (fm)					
		NN+3N–ind			NN+3N–full		
Nuclide	$\lambda_{\rm SRG}$ (fm^{-1})	Bare	2B	3B	Bare	2B	3B
^{4}He	1.88	1.48	1.47	1.46	1.42	1.40	1.39
	2.0	1.47	1.46	1.45	1.41	1.40	1.39
	2.24	1.46	1.45	1.45	1.39	1.39	1.38
^{16}O	1.88	2.32	2.29	2.26	2.28	2.24	2.22
	2.0	2.30	2.27	2.25	2.27	2.23	2.21
	2.24	2.28	2.25	2.24	2.25	2.22	2.20
^{40}Ca	1.88	2.91	2.89	2.85	2.86	2.83	2.79
	2.0	2.89	2.86	2.83	2.84	2.82	2.79
	2.24	2.84	2.82	2.80	2.83	2.80	2.78

body evolved, and three-body evolved mean-squared radius operators. As with the bare radius operator, we check the convergence pattern and find the root-mean-squared radius results converged within 0.01 fm. Evaluated charge radii are illustrated in Fig. 7. Final results for root-mean-squared radii from NN+3N–ind and $NN+3N$–full interactions are exhibited in Table II. For all nuclei, as we calculate with the higher-body evolved operator, the radii tend to become smaller and go away from the data. This behavior is consistent with the earlier NCSM results [36]. As was observed for the SRG induced three-body interaction, the consistently evolved operator moderately reduces the $\lambda_{\rm SRG}$-dependence of radii. Therefore, it can be concluded that the consistent SRG evolution of the radius operator does not give the significant change compared to the experimental data. This is consistent with the long-range nature of the radius operator [36]. In this work, we do not observe the enhancement of radii discussed in Ref. [63]. The quantitative reproduction of nuclear size is still an open question, and further investigations for nuclear interaction are indispensable. To examine and explore the nuclear Hamiltonian, feedbacks from many-body calculations for medium-mass systems can be a useful tool. Such studies are ongoing.

V. CONCLUSION

We have calculated the ground-state energies and radii for ^{4}He, ^{16}O, and ^{40}Ca with the UMOA using NN and 3N interactions based on χEFT for the first time. To obtain a computationally tractable Hamiltonian for the UMOA, we employed the SRG evolution and the NO2B approximation.

The resulting ground-state energies and radii agree with the recent *ab initio* calculation results within a few percent. Through the comparison with the MBPT, we discussed which contributions are taken into account in the UMOA. To improve the accuracy of the UMOA calculation, we need to take into account the many-body cluster terms. Following the systematic cluster expansion discussed in Ref. [33], an iterative treatment of the three-body cluster term is in progress. Also, this extension enables the direct inclusion of three-body interactions beyond the NO2B approximation. The results will be discussed in the future publication.

In addition to expectation values for the bare radius operator, we have investigated the two- and three-body SRG evolved radius operators. By taking higher-body evolved operators into account, calculated radii slightly shrink, while the $\lambda_{\rm SRG}$-dependence of radii is reduced as we keep up to three-body terms. Therefore, it is unlikely to reproduce the nuclear radii with the interactions employed in this work, even if we continue to include many-body terms induced by SRG evolution. The simultaneous reproduction of the ground-state energies and radii is still an open question.

ACKNOWLEDGMENTS

We thank R. Roth for providing us the coupled-cluster calculation results. This work was supported in part by JSPS KAKENHI Grant No. JP16J05707 and by the Program for Leading Graduate Schools, MEXT, Japan. This work was also supported in part by MEXT as "Priority Issue on post-K computer" (Elucidation of the Fundamental Laws and Evolution of the Universe), JICFuS (Projects No. hp160211 and No. hp170230), CNS-RIKEN joint project for large-scale nuclear structure calculations, the NSERC Grant No. SAPIN-2016-00033, and DOE Contract DE-FG02-97ER41014. TRIUMF receives

federal funding via a contribution agreement with the National Research Council of Canada. A part of numerical calculations were done on Oakforest-PACS, Supercomputing Division, Information Technology Center, the University of Tokyo.

Appendix A: Fourth order contributions in UMOA

Here, we present the connection between the UMOA and MBPT at fourth order. For the sake of simplicity, we work out with the HF basis which means off-diagonal matrix elements of one-body Hamiltonian are zero. At the fourth order of the MBPT, the contribution to the ground-state energy is

$$E^{[4]}_{\rm MBPT} = \sum_{i=1}^{39} F_i. \tag{A1}$$

Here, F_i corresponds to each diagram exhibited in Fig. 8. After the straightforward perturbative expansion, the fourth order contributions in the UMOA are

$$E^{[4]1,2{\rm BC}} = -F_5 - F_6 + F_{14} + F_{15} - F_{35} - F_{36}, \tag{A2}$$

$$E^{[4]3{\rm BC}} = 2(F_5 + F_6) + F_8 + F_9 + F_{10} + F_{11} - 4F_{15} + 2(F_{35} + F_{36}), \tag{A3}$$

$$E^{[4]}_{\rm UMOA} = F_5 + F_6 + F_8 + F_9 + F_{10} + F_{11} + F_{14} - 3F_{15} + F_{35} + F_{36}. \tag{A4}$$

While the hole-hole and particle-particle ladder type diagrams are included, the particle-hole and complicated topologies are missing in the UMOA. Since the difference between the UMOA and third-order HF-MBPT shown in Fig. 3 mainly comes from fourth order contributions taken into account in the UMOA, contributions $E^{[4]}_{1,2{\rm BC}}$, $E^{[4]}_{3{\rm BC}}$, and $E^{[4]}_{\rm UMOA}$ give repulsion. Comparison with the other methods is useful. According to Ref. [28], up to third order contributions are completed in CCSD, Λ-CCSD(T), and IM-SRG. The fourth order contributions in these methods are [28]

$$E^{[4]}_{\rm CCSD} = \sum_{i=1}^{16} F_i + \sum_{i=33}^{39} F_i, \tag{A5}$$

$$E^{[4]}_{\Lambda-{\rm CCSD(T)}} = \sum_{i=1}^{39} F_i, \tag{A6}$$

$$E^{[4]}_{\rm IM-SRG} = \sum_{i=1}^{16} F_i + F_{35} + F_{36} + F_{37} + \frac{1}{2}\left(F_{33} + F_{34} + F_{38} + F_{39}\right). \tag{A7}$$

Note that $E^{[4]}_{\rm IM-SRG}$ is obtained with IM-SRG(2) truncation.

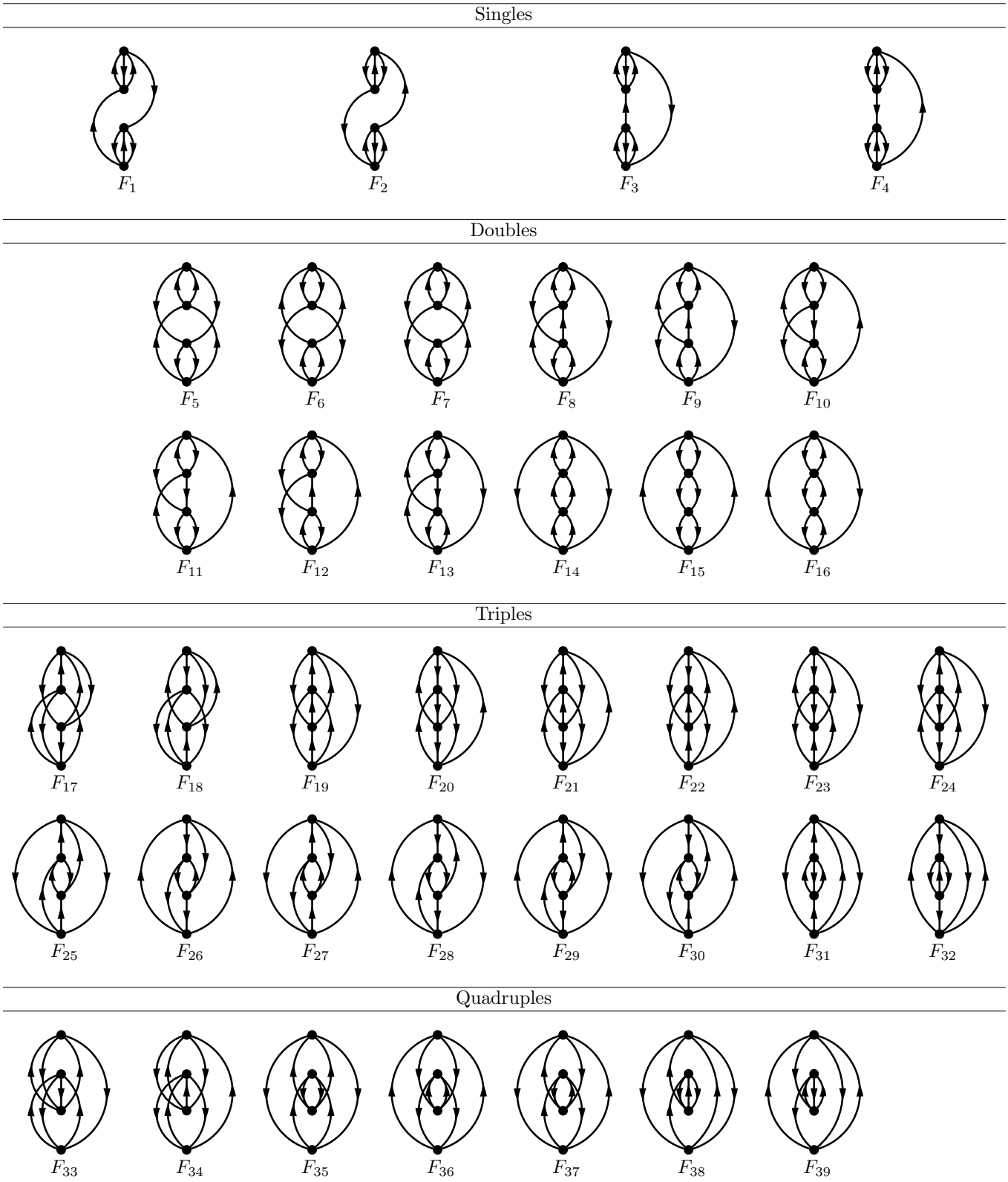

FIG. 8. Hugenholtz diagrams for the ground-state energy at the fourth order. The diagrams are classified into single, double, triple, and quadruple topologies, depending on the number of intermediate particle-hole excitations. The diagram rules are same as in Ref. [41].

[1] E. Epelbaum, H.-W. Hammer, and Ulf-G. Meißner, Rev. Mod. Phys. **81**, 1773 (2009), arXiv:0811.1338.

[2] R. Machleidt and D. Entem, Phys. Rep. **503**, 1 (2011), arXiv:1105.2919.

[3] S. Binder, A. Calci, E. Epelbaum, R. J. Furnstahl, J. Golak, K. Hebeler, H. Kamada, H. Krebs, J. Langhammer, S. Liebig, P. Maris, Ulf-G. Meißner, D. Minossi, A. Nogga, H. Potter, R. Roth, R. Skibiński, K. Topolnicki, J. P. Vary, and H. Witała, Phys. Rev. C **93**, 044002 (2016), arXiv:1505.07218.

[4] D. R. Entem, R. Machleidt, and Y. Nosyk, Phys. Rev. C **96**, 024004 (2017), arXiv:1703.05454.

[5] S. Binder, A. Calci, E. Epelbaum, R. J. Furnstahl, J. Golak, K. Hebeler, T. Hüther, H. Kamada, H. Krebs, P. Maris, Ulf-G. Meißner, A. Nogga, R. Roth, R. Skibiński, K. Topolnicki, J. P. Vary, K. Vobig, and H. Witała, Phys. Rev. C **98**, 014002 (2018), arXiv:1807.02848.

[6] P. Navratil, V. G. Gueorguiev, J. P. Vary, W. E. Ormand, and A. Nogga, Phys. Rev. Lett. **99**, 042501 (2007), arXiv:0701038 [nucl-th].

[7] G. Hupin, S. Quaglioni, J. Langhammer, P. Navrátil, A. Calci, and R. Roth, Few-Body Syst. **55**, 1013 (2014), arXiv:1401.0365.

[8] J. Langhammer, P. Navrátil, S. Quaglioni, G. Hupin, A. Calci, and R. Roth, Phys. Rev. C **91**, 021301(R) (2015), arXiv:1411.2541.

[9] G. Hupin, S. Quaglioni, and P. Navrátil, Phys. Rev. Lett. **114**, 212502 (2015), arXiv:1412.4101.

[10] T. Otsuka, T. Suzuki, J. D. Holt, A. Schwenk, and Y. Akaishi, Phys. Rev. Lett. **105**, 032501 (2010), arXiv:0908.2607.

[11] G. Hagen, M. Hjorth-Jensen, G. R. Jansen, R. Machleidt, and T. Papenbrock, Phys. Rev. Lett. **108**, 242501 (2012), arXiv:1202.2839.

[12] G. Hagen, M. Hjorth-Jensen, G. R. Jansen, R. Machleidt, and T. Papenbrock, Phys. Rev. Lett. **109**, 032502 (2012), arXiv:1204.3612.

[13] H. Hergert, S. Binder, A. Calci, J. Langhammer, and R. Roth, Phys. Rev. Lett. **110**, 242501 (2013), arXiv:1302.7294.

[14] H. Hergert, S. K. Bogner, S. Binder, A. Calci, J. Langhammer, R. Roth, and A. Schwenk, Phys. Rev. C **87**, 034307 (2013), arXiv:1212.1190.

[15] H. Hergert, S. K. Bogner, T. D. Morris, S. Binder, A. Calci, J. Langhammer, and R. Roth, Phys. Rev. C **90**, 041302(R) (2014), arXiv:1408.6555.

[16] V. Somà, A. Cipollone, C. Barbieri, P. Navrátil, and T. Duguet, Phys. Rev. C **89**, 061301(R) (2014), arXiv:1312.2068.

[17] A. Cipollone, C. Barbieri, and P. Navrátil, Phys. Rev. C **92**, 014306 (2015), arXiv:1412.0491.

[18] S. Binder, J. Langhammer, A. Calci, and R. Roth, Phys. Lett. B **736**, 119 (2014), arXiv:1312.5685.

[19] K. Hebeler, S. K. Bogner, R. J. Furnstahl, A. Nogga, and A. Schwenk, Phys. Rev. C **83**, 031301(R) (2011), arXiv:1012.3381.

[20] M. Kohno, Phys. Rev. C **88**, 064005 (2013) arXiv:1309.4556, Phys. Rev. C **96**, 059903(E) (2017).

[21] G. Hagen, T. Papenbrock, A. Ekström, K. A. Wendt, G. Baardsen, S. Gandolfi, M. Hjorth-Jensen, and C. J. Horowitz, Phys. Rev. C **89**, 014319 (2014), arXiv:1311.2925.

[22] I. Tews, S. Gandolfi, A. Gezerlis, and A. Schwenk, Phys. Rev. C **93**, 024305 (2016), arXiv:1507.05561.

[23] B. R. Barrett, P. Navrátil, and J. P. Vary, Prog. Part. Nucl. Phys. **69**, 131 (2013).

[24] J. Carlson, S. Gandolfi, F. Pederiva, S. C. Pieper, R. Schiavilla, K. E. Schmidt, and R. B. Wiringa, Rev. Mod. Phys. **87**, 1067 (2015), arXiv:1412.3081.

[25] D. Lee, Prog. Part. Nucl. Phys. **63**, 117 (2009), arXiv:0804.3501.

[26] G. Hagen, T. Papenbrock, M. Hjorth-Jensen, and D. J. Dean, Reports Prog. Phys. **77**, 096302 (2014), arXiv:1312.7872.

[27] W. Dickhoff and C. Barbieri, Prog. Part. Nucl. Phys. **52**, 377 (2004), arXiv:0402034 [nucl-th].

[28] H. Hergert, S. Bogner, T. Morris, A. Schwenk, and K. Tsukiyama, Phys. Rep. **621**, 165 (2016), arXiv:1512.06956.

[29] A. Tichai, J. Langhammer, S. Binder, and R. Roth, Phys. Lett. B **756**, 283 (2016), arXiv:1601.03703.

[30] B. S. Hu, F. R. Xu, Z. H. Sun, J. P. Vary, and T. Li, Phys. Rev. C **94**, 014303 (2016), arXiv:1604.07146.

[31] T. D. Morris, J. Simonis, S. R. Stroberg, C. Stumpf, G. Hagen, J. D. Holt, G. R. Jansen, T. Papenbrock, R. Roth, and A. Schwenk, Phys. Rev. Lett. **120**, 152503 (2018), arXiv:1709.02786.

[32] K. Suzuki and R. Okamoto, Prog. Theor. Phys. **92**, 1045 (1994).

[33] T. Miyagi, T. Abe, R. Okamoto, and T. Otsuka, Phys. Rev. C **96**, 054312 (2017), arXiv:1708.00177.

[34] S. K. Bogner, R. J. Furnstahl, and R. J. Perry, Phys. Rev. C **75**, 061001(R) (2007), arXiv:0611045 [nucl-th].

[35] V. Lapoux, V. Somà, C. Barbieri, H. Hergert, J. D. Holt, and S. R. Stroberg, Phys. Rev. Lett. **117**, 052501 (2016), arXiv:1605.07885.

[36] M. D. Schuster, S. Quaglioni, C. W. Johnson, E. D. Jurgenson, and P. Navrátil, Phys. Rev. C **90**, 011301(R) (2014), arXiv:1402.7106.

[37] M. D. Schuster, S. Quaglioni, C. W. Johnson, E. D. Jurgenson, and P. Navrátil, Phys. Rev. C **92**, 014320 (2015), arXiv:1304.5491.

[38] E. D. Jurgenson, P. Navrátil, and R. J. Furnstahl, Phys. Rev. Lett. **103**, 082501 (2009), arXiv:0905.1873.

[39] R. Roth, S. Binder, K. Vobig, A. Calci, J. Langhammer, and P. Navrátil, Phys. Rev. Lett. **109**, 052501 (2012), arXiv:1112.0287.

[40] S. Binder, J. Langhammer, A. Calci, P. Navrátil, and R. Roth, Phys. Rev. C **87**, 021303(R) (2013), arXiv:1211.4748.

[41] I. Shavitt and R. J. Bartlett, *Many - Body Methods Chem. Phys. MBPT Coupled-Cluster Theory* (Cambridge University Press, Cambridge, 2009).

[42] K. Suzuki, R. Okamoto, and H. Kumagai, Phys. Rev. C **36**, 804 (1987).

[43] K. Suzuki, Prog. Theor. Phys. **79**, 330 (1988).

[44] S. Ôkubo, Prog. Theor. Phys. **12**, 603 (1954).

[45] S. Lee and K. Suzuki, Phys. Lett. B **91**, 173 (1980).

[46] K. Suzuki and S. Y. Lee, Prog. Theor. Phys. **64**, 2091 (1980).

[47] K. Suzuki and R. Okamoto, Prog. Theor. Phys. **70**, 439 (1983).

[48] K. Suzuki and R. Okamoto, Prog. Theor. Phys. **72**, 534 (1984).

[49] K. Suzuki and R. Okamoto, Prog. Theor. Phys. **76**, 127 (1986).

[50] M. Wang, G. Audi, A. Wapstra, F. Kondev, M. MacCormick, X. Xu, and B. Pfeiffer, Chinese Phys. C **36**, 1603 (2012).

[51] D. R. Entem and R. Machleidt, Phys. Rev. C **68**, 041001(R) (2003), arXiv:0304018 [nucl-th].

[52] P. Navrátil, Few-Body Syst. **41**, 117 (2007), arXiv:0707.4680.

[53] R. Roth, A. Calci, J. Langhammer, and S. Binder, Phys. Rev. C **90**, 024325 (2014), arXiv:1311.3563.

[54] D. Gazit, S. Quaglioni, and P. Navrátil, Phys. Rev. Lett. **103**, 102502 (2009), arXiv:0812.4444, Phys. Rev. Lett. **122**, 029901(E) (2019).

[55] L. E. Marcucci, A. Kievsky, S. Rosati, R. Schiavilla, and M. Viviani, Phys. Rev. Lett. **108**, 052502 (2012), arXiv:1109.5563, Phys. Rev. Lett. **121**, 049901(E) (2018).

[56] S. Binder, P. Piecuch, A. Calci, J. Langhammer, P. Navrátil, and R. Roth, Phys. Rev. C **88**, 054319 (2013), arXiv:1309.1123.

[57] A. Cipollone, C. Barbieri, and P. Navrátil, Phys. Rev. Lett. **111**, 062501 (2013), arXiv:1303.4900v1.

[58] I. Angeli and K. Marinova, At. Data Nucl. Data Tables **99**, 69 (2013).

[59] J. L. Friar and J. W. Negele, Adv. Nucl. Phys. **8**, 219 (1975).

[60] C. Patrignani, K. Agashe, G. Aielli, C. Amsler, M. Antonelli, D. M. Asner, H. Baer, S. Banerjee, R. M. Barnett, T. Basaglia, C. W. Bauer, J. J. Beatty, V. I. Belousov, J. Beringer, S. Bethke, H. Bichsel, O. Biebel, E. Blucher, G. Brooijmans, O. Buchmueller, V. Burkert, M. A. Bychkov, R. N. Cahn, M. Carena, A. Ceccucci, A. Cerri, D. Chakraborty, M. C. Chen, R. S. Chivukula, K. Copic, G. Cowan, O. Dahl, G. D'Ambrosio, T. Damour, D. De Florian, A. De Gouvêa, T. DeGrand, P. De Jong, G. Dissertori, B. A. Dobrescu, M. D'Onofrio, M. Doser, M. Drees, H. K. Dreiner, D. A. Dwyer, P. Eerola, S. Eidelman, J. Ellis, J. Erler, V. V. Ezhela, W. Fetscher, B. D. Fields, B. Foster, A. Freitas, H. Gallagher, L. Garren, H. J. Gerber, G. Gerbier, T. Gershon, T. Gherghetta, A. A. Godizov, M. Goodman, C. Grab, A. V. Gritsan, C. Grojean, D. E. Groom, M. Grünewald, A. Gurtu, T. Gutsche, H. E. Haber, K. Hagiwara, C. Hanhart, S. Hashimoto, Y. Hayato, K. G. Hayes, A. Hebecker, B. Heltsley, J. J. Hernández-Rey, K. Hikasa, J. Hisano, A. Höcker, J. Holder, A. Holtkamp, J. Huston, T. Hyodo, K. Irwin, J. D. Jackson, K. F. Johnson, M. Kado, M. Karliner, U. F. Katz, S. R. Klein, E. Klempt, R. V. Kowalewski, F. Krauss, M. Kreps, B. Krusche, Y. V. Kuyanov, Y. Kwon, O. Lahav, J. Laiho, P. Langacker, A. Liddle, Z. Ligeti, C. J. Lin, C. Lippmann, T. M. Liss, L. Littenberg, K. S. Lugovsky, S. B. Lugovsky, A. Lusiani, Y. Makida, F. Maltoni, T. Mannel, A. V. Manohar, W. J. Marciano, A. D. Martin, A. Masoni, J. Matthews, U. G. Meißner, D. Milstead, R. E. Mitchell, P. Molaro, K. Mönig, F. Moortgat, M. J. Mortonson, H. Murayama, K. Nakamura, M. Narain, P. Nason, S. Navas, M. Neubert, P. Nevski, Y. Nir, K. A. Olive, S. Pagan Griso, J. Parsons, J. A. Peacock, M. Pennington, S. T. Petcov, V. A. Petrov, A. Piepke, A. Pomarol, A. Quadt, S. Raby, J. Rademacker, G. Raffelt, B. N. Ratcliff, P. Richardson, A. Ringwald, S. Roesler, S. Rolli, A. Romaniouk, L. J. Rosenberg, J. L. Rosner, G. Rybka, R. A. Ryutin, C. T. Sachrajda, Y. Sakai, G. P. Salam, S. Sarkar, F. Sauli, O. Schneider, K. Scholberg, A. J. Schwartz, D. Scott, V. Sharma, S. R. Sharpe, T. Shutt, M. Silari, T. Sjöstrand, P. Skands, T. Skwarnicki, J. G. Smith, G. F. Smoot, S. Spanier, H. Spieler, C. Spiering, A. Stahl, S. L. Stone, Y. Sumino, T. Sumiyoshi, M. J. Syphers, F. Takahashi, M. Tanabashi, K. Terashi, J. Terning, R. S. Thorne, L. Tiator, M. Titov, N. P. Tkachenko, N. A. Törnqvist, D. Tovey, G. Valencia, R. Van De Water, N. Varelas, G. Venanzoni, M. G. Vincter, P. Vogel, A. Vogt, S. P. Wakely, W. Walkowiak, C. W. Walter, D. Wands, D. R. Ward, M. O. Wascko, G. Weiglein, D. H. Weinberg, E. J. Weinberg, M. White, L. R. Wiencke, S. Willocq, C. G. Wohl, L. Wolfenstein, J. Womersley, C. L. Woody, R. L. Workman, W. M. Yao, G. P. Zeller, O. V. Zenin, R. Y. Zhu, F. Zimmermann, P. A. Zyla, J. Anderson, G. Harper, V. S. Lugovsky, and P. Schaffner, Chinese Phys. C **40**, 100001 (2016).

[61] A. Ekström, G. R. Jansen, K. A. Wendt, G. Hagen, T. Papenbrock, B. D. Carlsson, C. Forssén, M. Hjorth-Jensen, P. Navrátil, and W. Nazarewicz, Phys. Rev. C **91**, 051301(R) (2015), arXiv:1502.04682.

[62] J. Simonis, S. R. Stroberg, K. Hebeler, J. D. Holt, and A. Schwenk, Phys. Rev. C **96**, 014303 (2017), arXiv:1704.02915.

[63] G. A. Miller, A. Beck, S. M.-T. Beck, L. B. Weinstein, E. Piasetzky, and O. Hen, arXiv:1805.12099.

[64] T. Miyagi, T. Abe, R. Okamoto, and T. Otsuka, Prog. Theor. Exp. Phys. **2015**, 041D01 (2015), arXiv:1504.04965.

[65] D. Lonardoni, A. Lovato, S. C. Pieper, and R. B. Wiringa, Phys. Rev. C **96**, 024326 (2017), arXiv:1705.04337.